Coseismic Groundwater Drawdown Along Crustal Ruptures During the 2016 M_w 7.0 Kumamoto Earthquake

T. Hosono[1], C. Yamada[1], T. Shibata[2], Y. Tawara[3], C.-Y. Wang[4], M. Manga[4], A. T. M. S. Rahman[1], and J. Shimada[1]

[1] Department of Earth and Environmental Science, Kumamoto University, Kumamoto, Japan, [2] Institute for Geothermal Sciences, Kyoto University, Oita, Japan, [3] Geosphere Environmental Technology Corporation, Tokyo, Japan, [4] Department of Earth and Planetary Science, University of California, Berkeley, CA, USA

Correspondence to: T. Hosono, hosono@kumamoto-u.ac.jp

Abstract

Groundwater-level changes after earthquakes provide insight into changes in hydrogeological properties such as permeability and pore pressure. Quantifying such changes, both their location and magnitude, is usually hindered by limited data. Using extensive high-resolution water-level monitoring records, we provide direct evidence of significant groundwater drawdown (4.74-m maximum) over a 160-km^2 area along crustal ruptures after the M_w 7.0, 2016, Kumamoto earthquake. Approximately 10^6 m^3 of water disappeared within 35 min after the main shock. The loss of water was not caused by static-strain driven pore-pressure decrease nor by releasing of water through structural pathways, but most likely by water transfer downwards through open cracks. Such changes may impact the security of water resources, the safety of underground waste repositories, and contaminant transport in seismically active areas.

1 Introduction

Changes in spring discharge and groundwater levels associated with large earthquakes have been recognized for more than 2,000 years (Pliny, the Elder, ca. AD 77-79n.d.). The principal mechanisms invoked to explain these hydrological changes include pore-pressure response to coseismic static elastic strain (e.g., Jónsson et al., 2003; Muir-Wood & King, 1993; Wakita, 1975), permeability changes caused by seismic waves (e.g., Elkhoury et al., 2006; Rojstaczer & Wolf, 1992; Wang et al., 2004), and fluid migration along seismogenic dilatant cracks or crustal ruptures (e.g., Sibson & Rowland, 2003; Tsunogai & Wakita, 1995; Wang et al., 2001). In contrast to coseismic strain and seismic wave-induced hydrological responses that are detectable thousands of kilometers from earthquake epicenters (e.g., Brodsky et al., 2003; Montgomery & Manga, 2003; Shi et al., 2015), in situ hydrological alterations in the vicinity of active fault systems are poorly understood because of limited data. Here we present observations from a high-resolution monitoring network in the near field of the Kumamoto earthquake rupture area.

A lake fed by springs (Lake Suizenji) emptied within 4 hr of the main shock of the 2016 Kumamoto earthquake (M_w 7.0, 01:25 Japan standard time [JST], 16 April 2016; Figure 1). A high-resolution groundwater monitoring network was in place at Kumamoto at the time of the earthquake (Figure 1a; see section 3) with a spatial resolution that is more than 3 and 15 times finer than those documenting the effects of the 1999 Chi-Chi (Manga & Wang, 2015) and the 2010 Canterbury (Cox et al., 2012) earthquakes, respectively. The data set thus provides an excellent opportunity to directly document groundwater responses along newly formed rupture systems (Figure 1b; Fujiwara et al., 2016; Goto et al., 2017).

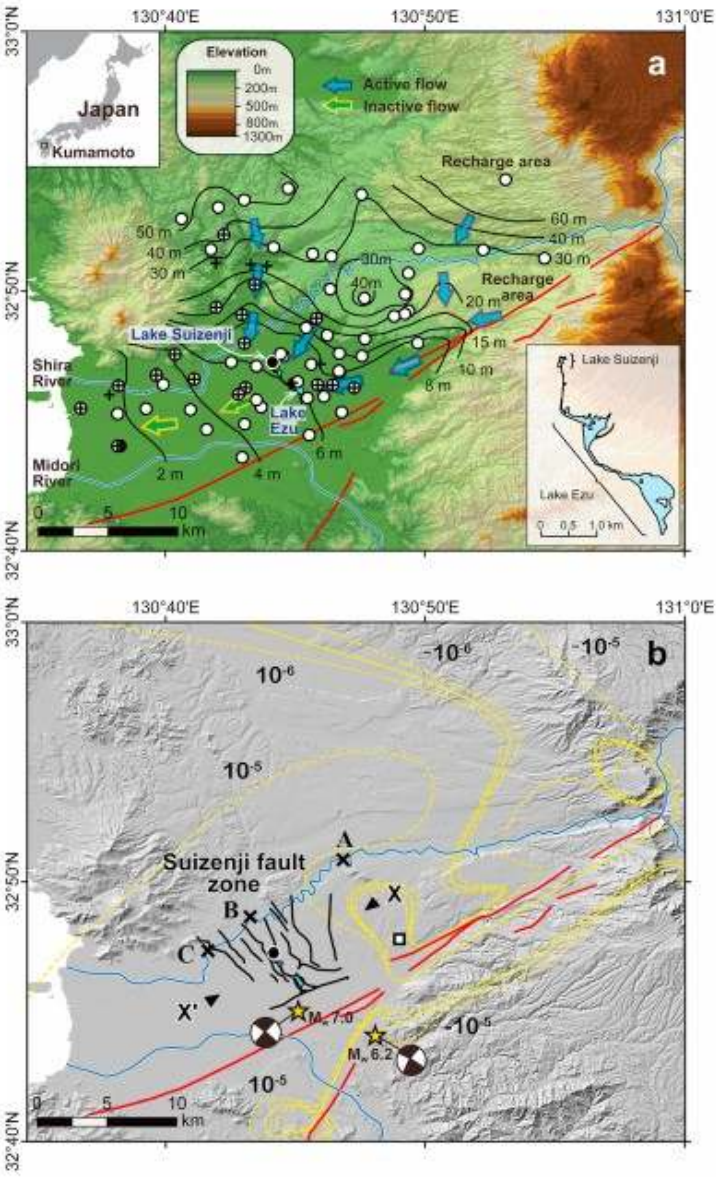

Figure 1. Groundwater flow and tectonic map. (a) Groundwater potential contour map for the confined aquifer before the 2016 Kumamoto earthquake sequence (21:00 Japan standard time [JST], 14 April 2016). Arrows in the figure show the directions and characteristics of groundwater flows (see details in the text). The locations of groundwater monitoring wells recording coseismic water-level changes used in this study are shown for unconfined (cross) and confined (open circle) aquifers, respectively. There are two different wells (for confined and unconfined aquifers) in the same site for some locations (cross inside open circle). Location of Lake Suizenji is shown with the solid circle. The shapes of spring-fed lakes are outlined in the right-bottom corner. (b) Map showing tectonic structures: a newly recognized fault system (Suizenji fault zone; black lines) appeared after the main shock to the north of the pre-existing active Futagawa and Hinagu faults (red lines). The new faults crosscut metrologically driven water flow system. The position of the foreshock (21:26 JST, 14 April 2016, M_w 6.2, focal depth = 11 km) and main shock epicenters (01:25 JST, 16 April 2016, M_w 7.0, focal depth = 12 km) are shown with stars. Coseismic volumetric strain calculated at a depth of 100 m is shown with yellow contours. The spring-fed lake in Suizenji (ca. 8,500 m^3/day average annual flux, 0.5-m maximum depth) dried up after the main shock. The labels A, B, and C in the Shira River represent monitoring gauges for river water level (see Figure 5). Open square shows the location of seismic station KMMH16 (see section 5). Coseismic hydrogeological changes model cross-section X-X′ is shown in Figure 6.

2 Study Area and the 2016 Kumamoto Earthquake

The Kumamoto region is characterized hydrologically by active groundwater flows within Quaternary volcanic pyroclastic deposits, porous lava, and alluvial deposits (Figure 1a; Hosono et al., 2013, and references therein). Two major aquifer systems are separated by an impermeable aquitard, with an unconfined aquifer (approximately <50 m in depth) overlying a confined

aquifer (approximately 60–200 m). Both aquifers are mostly recharged through highly permeable volcanic deposits in the northern and eastern highlands (Figure 1a). These near-surface groundwater systems represent the upper 200 m that overlie relatively impermeable basement of Paleozoic metasedimentary rocks and Pliocene to Quaternary volcanic rocks. Groundwater flows laterally southward and westward along the topographical gradient, and mostly discharges within 40 years as springs in Lake Ezu (0.57 km^2, 2.6-m maximum depth; see Figure 1a for locations) at the entrance of the surrounding plains (see Hosono et al., 2013; Kagabu et al., 2017; and Ono et al., 2013, for more detailed hydrogeological descriptions of the study area). Lake Suizenji (Figure 1a) is one of the spring sources feeding Lake Ezu. However, some stagnant groundwater remains in the plain and coast in soft marine clay (~60-m thickness) deposited at the time of the last marine transgression.

The groundwater systems and the monitoring network are located to the northwest of the pre-existing active Futagawa and Hinagu faults (red lines in Figure 1). The 2016 Kumamoto earthquake sequence involved strike-slip and normal displacement, with a northwest-southeast extension and focal depths of 3–17 km (e.g., Sano et al., 2016). The sequence began with a M_w 6.2 foreshock on 14 April, followed by the M_w 7.0 main shock on 16 April. Importantly, the main shock reveals newly recognized postseismic fault systems called the Suizenji fault zone (Fujiwara et al., 2016; Goto et al., 2017) and crosscut groundwater flow systems and the Shira River, the main river within studied catchment (Figure 1). These faults were formed by large ($>10^{-5}$) extensional volumetric strain (Figure 1b). Numerous aftershocks occurred along these fault systems (see Fujiwara et al., 2016, and Goto et al., 2017, for their locations). In this study, special emphasis is placed on the co-location between the new rupture systems and the coseismic groundwater changes (Figure 2) to understand how the crustal deformation can induce the observed water-level changes.

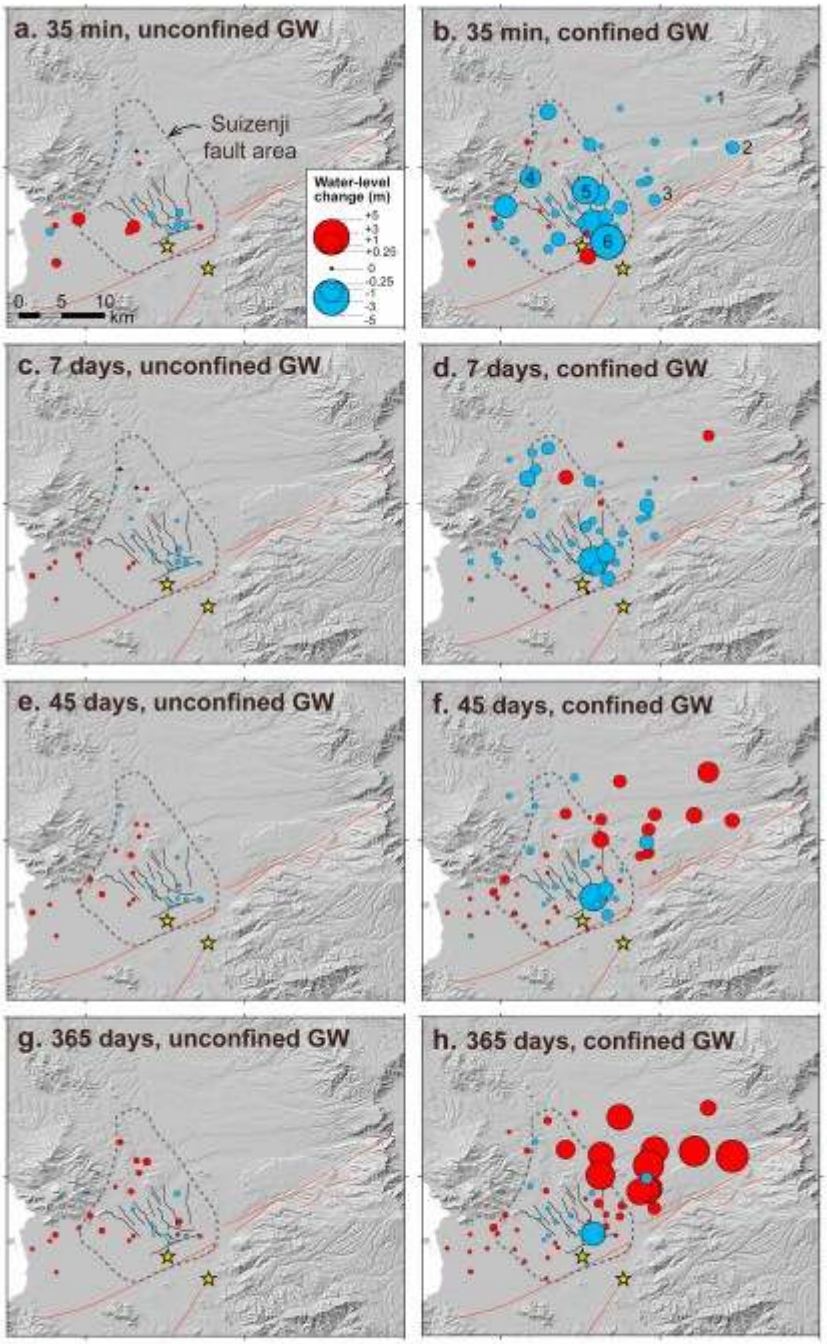

Figure 2. Spatiotemporal changes of water levels. (a to h) Relative water-level changes comparing water levels before the Kumamoto earthquake sequence (21:00 Japan standard time [JST], 14 April 2016) and 35 min, 7 days, 45 days, and 365 days after the main shock (01:25 JST, 16 April 2016) for unconfined and confined aquifers. The Suizenji fault area is shown as a dashed line. Earthquake epicenters and fault systems are as depicted in Figure 1. Numbers (1 to 6) labeled in or beside the plots in Figure 2b correspond the well numbers in Figure 3 showing detailed water-level change time series.

3 Methods

3.1 Groundwater-Level Data

Kumamoto is a city with about one million people that depends entirely on groundwater for drinking purposes (Hosono et al., 2013; Taniguchi et al., 2019, and references therein). The groundwater is mostly derived from the confined aquifer. For this reason, a large number of groundwater monitoring wells, especially for confined aquifer systems, is installed by government agencies within an area of 300 km^2. However, the number of wells is limited for unconfined aquifers especially in eastern recharge area (Figure 1). Among the 113 wells, 21 monitoring wells could not be used as data sources because of direct mechanical damage and data loss caused by the earthquake, leaving us with useful data from 92 wells (see Figure 1a for their distributions). Groundwater levels are recorded with a float-type meter or a pressure sensor and archived hourly as digital data. Thus, the record at 02:00 JST on 16 April 2016 is the first water-level measurement after the main shock (01:25 JST on 16 April 2016), 35 min after the earthquake. We obtained analogue chart recordings of water level for some wells where float-type meters are installed. The chart displayed finer time resolution for water-level changes than the digital ones, especially on the first day after the main shock. In this study we used digital data since the number of wells recording analogue data was small.

Water levels are recorded as elevation (m) above sea level. These elevations are obtained by simple subtraction of measured distance (m) between the ground surface and water head from ground surface elevation above sea level. We need to account for changes in ground surface elevation after the earthquake to obtain accurate water-level elevation. Vertical ground level changes were estimated using interferometric synthetic aperture radar data provided by the Geospatial Information Authority of Japan (http://www.gsi.go.jp/BOUSAI/H27-kumamoto-earthquake-index.html), and we used these data to recalculate water levels after the main shock. Horizontal surface land displacements are reported on the same website.

3.2 Volumetric Static Strain

Volumetric static strains were calculated with an elastic dislocation model (Okada, 1992) using fault displacements inverted from interferometric synthetic aperture radar satellite and global navigation satellite system data (Yarai et al., 2016). The data were inverted with uniform slip on four rectangular faults in an elastic half-space for the two main foreshocks and mainshock in the 2016 Kumamoto earthquake sequence. The map showing calculated changes in volumetric strain (Figure 1b) was computed at a depth of 100 m below surface, which corresponds approximately to the middle of the aquifers, and was drawn using Generic Mapping Tools (Wessel & Smith, 1998). Point data at the screen level or well depth (if there is no screen level data) of each well were estimated from the independent dataset (see Table S1 in the supporting information). We understand that large discrepancies can occur between the observed volumetric strains and the predictions from the dislocation model (Wang & Barbour, 2017), but no measured volumetric strain before or after the earthquake is available in the studied area. We use

the dislocation model here to test if it may explain the observed water-level change in the study area.

3.3 Numerical Simulation

The GETFLOWS simulator (GEneral purpose Terrestrial fluid-FLOW Simulator), an integrated watershed modeling tool (Mori et al., 2015), was used for the numerical simulation in this study. The transport processes of water, air, various dissolved and volatilized materials, suspended sediments in water, and heat from the surface to the underground in arbitrary temporal-spatial scales are treated simultaneously in the GETFLOWS system. Governing equations are based on the mass and energy conservation. Fluid flow system is generalized as an air-water two-phase flow. The interaction between the fluid phases is considered except in surface environments where the gas phase is treated as an infinitely mobile fluid. Manning's law is applied with a diffusive wave approximation of the two-dimensional Saint Venant equations to compute the velocity field for surface water flow, while the generalized Darcy's law is employed for subsurface fluid flows and surface-subsurface fluid interaction to describe the fluid velocity field. An integral finite difference method is employed for spatial discretization to ensure local mass balance, and a fully implicit time discretization is employed to achieve stable computation. This simulator has been verified by many analytical solutions, controlled laboratory data, and more than 500 field data in Japan and overseas to ensure its accuracy and applicability (e.g., Kitamura et al., 2016; Mori et al., 2015; Sakuma et al., 2017; Tawara et al., 2014).

Detailed conditions and parameters used to validate the GETFLOWS modeling in the study area are provided in the supporting information including boundary conditions (Figure S1 in the supporting information), model grids and discretized geology (Figures S2 and S3), cross sections of the model domain (Figure S4), and input hydrologic and hydrogeologic parameters with data sources (Tables S2 and S3). Briefly, the simulated region encompasses an area of 2,689 km^2 fully covered hydrological systems of the study area (Figure S1). The number of grid blocks in the horizontal plane was 33,274. In the vertical direction, atmospheric and surface layers were used to set the boundary conditions with meteorological data and to simulate surface water flows. Additionally, the subsurface geology was discretized into 28 layers of variable thickness, and thus, the total number of grid blocks was 998,220 (Figures S2 and S3). The numerical model required data on meteorology, land use, elevation, surface soil, subsurface geology, and water use (Tables S2 and S3). The meteorological data included precipitation and air temperature, which were used to evaluate evapotranspiration and snowmelt. The land use classification was used to determine Manning's roughness coefficient. The surface soils and subsurface geology are associated with hydraulic parameters estimated from well tests such as permeability, effective porosity, and two-phase flow properties (Tables S2 and S3). Groundwater pumping, water intake from rivers, and rice paddy irrigation are included in the water use data. The time-dependent

evolution of hydrological conditions is computed using daily meteorological and water use. The model was validated by trial and error calibrations manually through comparisons with observed data (e.g., Figure S5): flow rates of 24 rivers, groundwater levels for 42 wells, total volume of spring water discharge to Lake Ezu for more than 5 years, temperature, and hydrochemical and isotopic parameters such as ^{3}H, $\delta^{18}O$, ^{85}Kr, and NO_3^- for groundwater from the monitoring wells (Hosono et al., 2013; Ichiyanagi et al., 2012; Mori et al., 2016; Shimada et al., 2012).

4 Observations

Before discussing coseismic water-level changes, two factors (seasonal water-level changes and coseismic ground-level changes) need to be considered. First, water levels in the study area are most constant during the months of April and May when water levels are lowest. For example, in 2015 the changes were between 0.05 and 0.86 m for all monitored wells (median value = 0.20 m, standard deviation = 0.18 m, n = 107). After the main shock, the water-level changes were significantly larger than seasonal changes for each well. Second, the levels of the well pipe heads were altered: ground levels dropped by a maximum of 2.0 m north of the Futagawa fault and rose by a maximum of 1.0 m south of the fault. We used interferometric synthetic aperture radar data to estimate ground-level changes and then to recalculate groundwater levels (see section 3). In this study, we used data from April and May 2016 and April 2017, 1 year after the main shock (Figure 2). All data are provided in Table S1 that includes locations, properties, groundwater levels, and computed volumetric static strain at each screened depth for all wells.

The results show dramatic spatiotemporal changes in groundwater levels after the main shock (Figures 2 and 3). The water-level drop peaked immediately after the main shock (within 35 min) for both the confined and unconfined aquifers with a maximum water drop of 4.74 m in central part of the study area (Figures 2a and 2b) where a newly recognized fault system developed. This water-level drop largely recovered within 45 days toward the background level through the annual hydrologic cycle (Figure 2). Local citizen newspapers reported that Lake Suizenji emptied within 4 hr of the main shock (https://mainichi.jp/english/articles/20160426/p2a/00m/0na/012000c). However, the water level in the lake recovered within 30 days of the main shock (information available only in Japanese: https://mainichi.jp/articles/20170529/ddl/k43/040/182000c). Both aquifer and spring water-level changes have similar temporal changes near the fault zone (Figure 1). There are no recorded time series of discharge that allow us to evaluate coseismic changes in the volumes of Lake Suizenji.

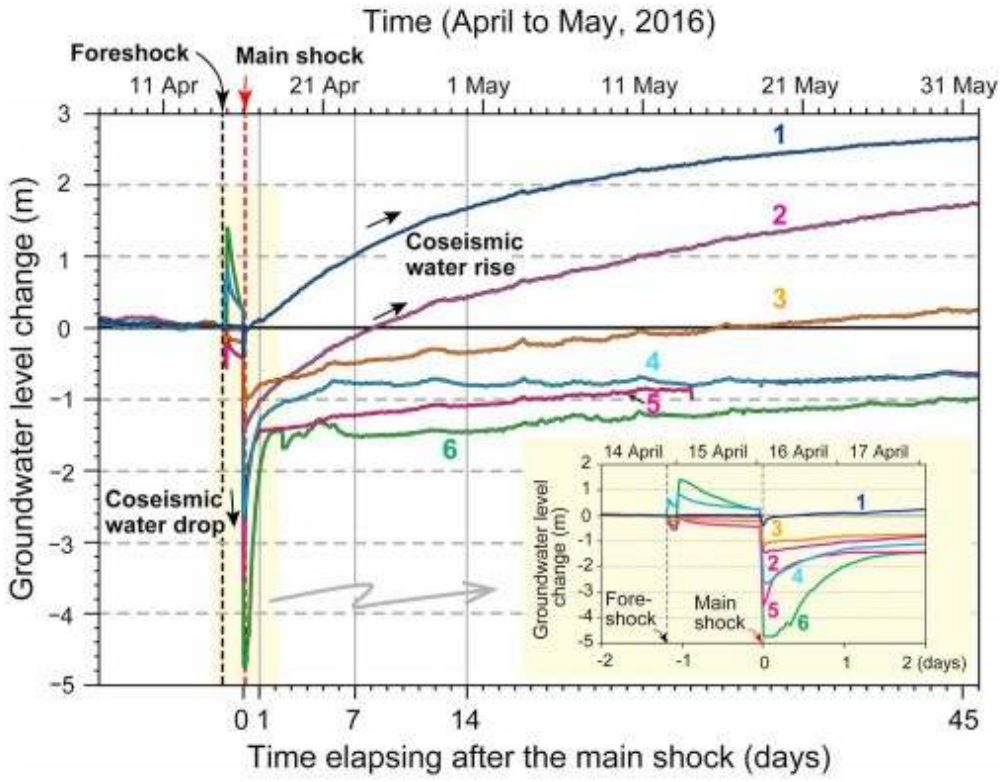

Figure 3. Water level change time series for selected wells. Postearthquake water-level changes relative to the water levels before the earthquake (21:00 Japan standard time [JST], 14 April 2016) during the first 45 days after the main shock of the 2016 Kumamoto earthquake for selected wells for the confined aquifer are shown using hourly monitored digital data. Zoom of the two days before and after the main shock is shown in lower right. The numbers in the figure (1 to 6) correspond the well numbers shown in Figure 2b.

In contrast, the water level rose in unconfined aquifers in the western coastal area immediately after the main shock (Figure 2), and, most significantly, in the eastern recharge area that initially dropped but then rose significantly above preearthquake levels 1 to 2 weeks after the main shock (Figures 2 and 3). The water levels in eastern areas continuously increased through the annual hydrologic cycle (Figure 2h). Some postseismic fault systems also crosscut eastern high-elevation mountains (Fujiwara et al., 2016), and increasing contributions of waters from these mountains into down slope aquifer systems are identified by isotopic fingerprints. Thus, we suggest that the observed water-level rise in eastern recharge areas is caused by coseismic mountain water release due to permeability enhancement (Jónsson et al., 2003; Wang et al., 2004; Wang & Manga, 2015). In this paper we focus on the mechanism of the observed groundwater drops after the main shock; water-level changes in response to the foreshock and water-level rises after the main shock require additional data and analysis and will be discussed elsewhere.

5 Discussion

5.1 Water Drawdown Mechanism

Water drops occurred within 35 min after the main shock in both aquifers (Figures 2a, 2b, and 3). However, after the initial drops the water levels tended to recover to the preearthquake values (Figures 2c-2h and 3). The three major suggested causes of coseismic water-level drops are extensional elastic static-strain (Jónsson et al., 2003; Muir-Wood & King, 1993; Wakita, 1975), increase in permeability from seismic vibration (Elkhoury et al., 2006; Mohr et al., 2017; Rojstaczer & Wolf, 1992; Wang et al., 2004), and fluid transfer along seismogenic dilatant cracks or crustal ruptures (Sibson & Rowland, 2003; Wang et al., 2001). If the static elastic volumetric strain explains the changes, there should be a good correlation between volumetric strain and water-level change. However, we find no such correlation for either the unconfined ($R^2 = 0.075$, $P = 0.23$, $n = 19$) or the confined ($R^2 = 0.024$, $P = 0.29$, $n = 52$) aquifers in the study area (Figure 4). The observations thus do not support the coseismic elastic strain model as the cause of observed water drops. On the other hand, this does not mean that volumetric strain is not important in the present study. Volumetric strain caused by factors not considered in the dislocation model, such as nonelastic deformation and pore pressure change, may be important in affecting the coseismic change of water level in the study area, as explained later.

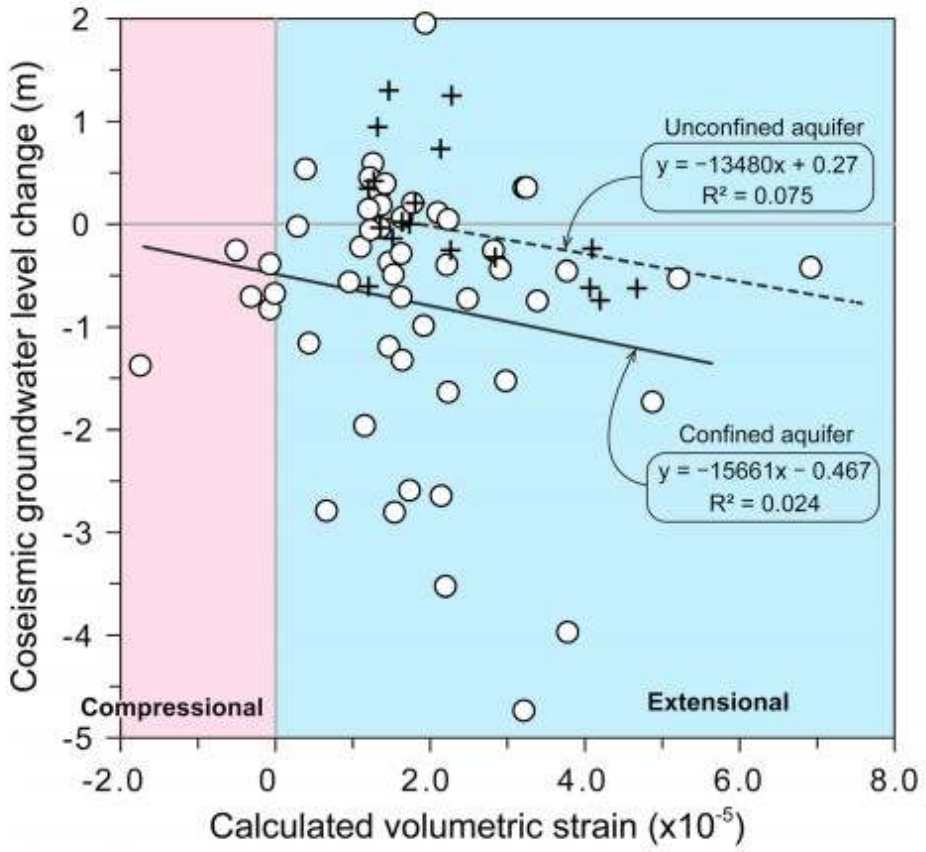

Figure 4. Relationship between coseismic water drop and calculated volumetric strain. Results for all wells 35 min after the main shock (Figures 2a and b) are shown for unconfined (cross; n =19) and confined aquifers (circle; n = 52), respectively, where we could obtain water-level data. Volumetric strain was calculated at each screen level. Note that there are no significant correlations between observed water drop and volumetric strain for both aquifers.

There are many reports of coseismic water-level drops attributed to an increase in permeability by seismic vibration accompanied by increased stream discharge (e.g., Rojstaczer et al., 1995; Sato et al., 2000). Around the Suizenji fault zone all water levels (for confined and unconfined aquifers and surface springs) dropped dramatically within few hours after the main shock (Figure 2); however, river gauge stations “B” and “C” (see Figure 1b for locations) showed no simultaneous increases in stream discharge in the main river (Shira River) in the fault zone (Figure 5). At the river gauge station “A” (Figures 1b), a site before the Shira River flows into fault zone, the water level increased immediately after the main shock (Figure 5), possibly due to the coseismic mountain water release in the upstream catchment (Wang et al., 2004; Wang & Manga, 2015). Destruction of an inlet channel from the upstream Shira River used for irrigation may also have caused water discharge to increase in the first few hours. However, at the river gauge stations B and C, the sites where the river crossed fault zone (Figure 1b), the water levels decreased in the first 12 hr after the main shock (Figure 5). There are no outlet channels between gauge stations A and C. Thus, water

must have leaked from the river into the fault zone. At about 12 hr after the main shock, the water levels rose at all stations as river discharge was increasingly fed by the released mountain waters and precipitation in the upstream catchment.

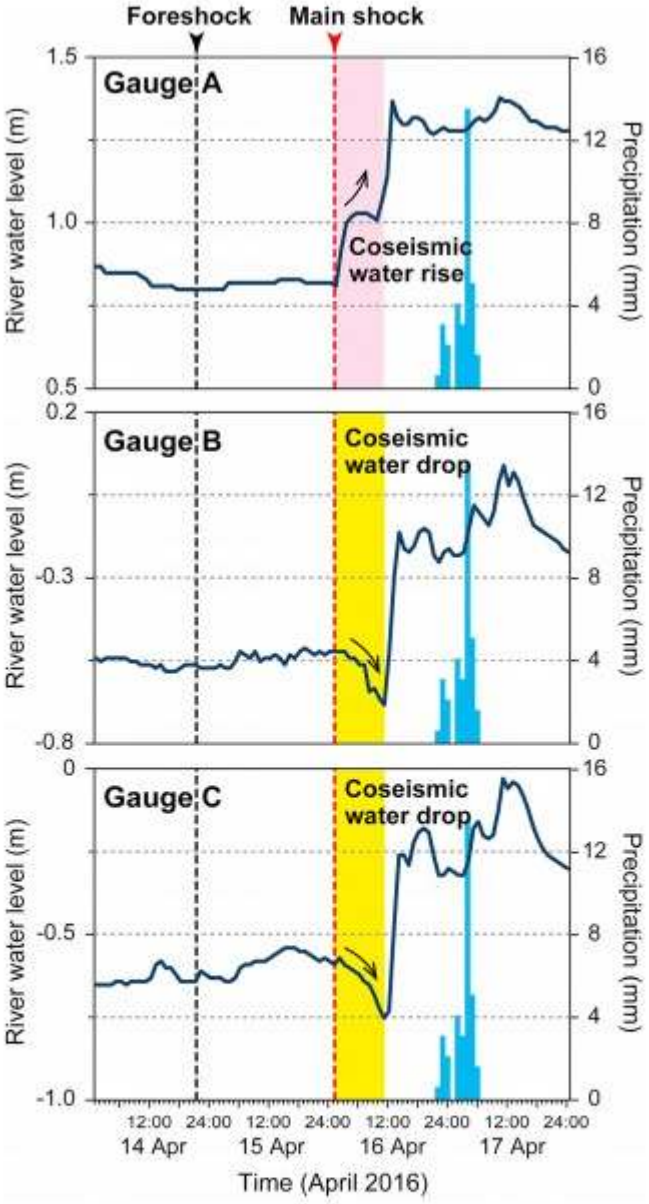

Figure 5. River water-level change time series. Data for three monitoring gauges, A, B, and C, are shown (data source: http://www1.river.go.jp/) during 2 days before and after the main shock of the 2016 Kumamoto earthquake. Obtained water-level data are described as "relative values" but not as absolute values. The monitoring gauge A is located at upstream of the Suizenji fault system, and gauges B and C are located in the middle and downstream of the fault system, respectively (see Figure 1b for their locations). Hourly records of precipitation within the catchment area (station Minamiaso) are shown with the bar graphs (data source: http://www1.river.go.jp/).

The water-level rise in unconfined aquifers in the plain and coastal area just after the main shock may be caused by in situ liquefaction or consolidation of sediments (Lai et al., 2004; Wakamatsu et al., 2017). Based on previous well-constrained regional groundwater flow models (Hosono et al., 2013; Kagabu et al., 2017; Ono et al., 2013), the area with water-level decreases is a groundwater discharge zone with significant upward flux. Water-level rise would thus be expected if aquifer permeability and thus groundwater flow rate increased due to seismic vibration.

We thus propose that downward fluid movement is a likely cause of the water-level drops. Three scenarios may be proposed to explain the observed water-level drops. First, water level may drop due to the release of the water from confined aquifers to the surface along crustal ruptures. The second hypothesis is that water replenishes deep crustal ruptures by low pressures generated during the formation of structural open spaces (Feuillet et al., 2011; Sibson & Rowland, 2003). The third hypothesis is that water replenishes dilatant cracks produced by strong seismic shaking (Wang et al., 2001). Evidence in support of the first scenario, such as coseismic surface water response in the form of spike increase in discharge, emergence of new springs, or increase in spring lake water discharges, were not found except some localized liquefaction. It is possible that the missing water might have been lost to the coastal area and out-flow to the sea via the Futagawa and Hinagu active faults (red lines in Figure 1). This possibility cannot be dismissed because we do not have observational data to quantify the coseismic submarine groundwater discharge. However, if this idea is correct, the groundwater-dropped area would have been localized along the NE-SW trending Futagawa fault due to permeability increase in shear zone, which is not the case in the studied area. Thus, we conclude that there is no plausible evidence to support the first scenario.

In contrast, the possibility of transporting fluids though crustal ruptures and/or dilatant cracks remains plausible. The Suizenji fault system (Fujiwara et al., 2016; Goto et al., 2017) was formed by crustal displacement under strong extensional stress (Figure 1b) permitting such pathways to form. Direct field evidence supporting this hypothesis is limited, though ongoing research on the groundwater hydrochemistry and microbiology in the Suizenji fault zone suggests mixing between the two main aquifers after the main shock and may ultimately support or refute this hypothesis. To further assess this hypothesis, we next analyze currently available fine-scale structural and water-level datasets from Kumamoto. To this end, we have defined the area of water-level drops around the Suizenji fault zone as the “Suizenji fault area” (Figure 2), which includes hypothesized subsurface fault systems.

5.2 Water Drop Estimates

The 2016 Kumamoto crustal earthquake sequence occurred with a large inelastic strain-rate ($>10^{-7}$ $year^{-1}$; Matsumoto et al., 2016), resulting in an

enormous number of aftershocks along the Futagawa and Hinagu active faults at a depth of ~17 km and under the Suizenji fault area at ~10 km (Goto et al., 2017; Yano & Matsubara, 2017). These seismotectonic features imply that the crustal materials are inelastic and deformation extends from near the surface down to several kilometers in the vicinity of faults. Normal faulting and graben-like features of the Suizenji fault system (Fujiwara et al., 2016; Goto et al., 2017) associated with eastward surface displacement to the east of the fault zone (~1.5 m; see section 3 for data source) may help to create the open cracks in the upper crust. It is difficult, however, to directly observe new cracks from geological observations. Therefore, we test the second hypothesis that low pressure was generated coseismically in new cracks (Figure 6).

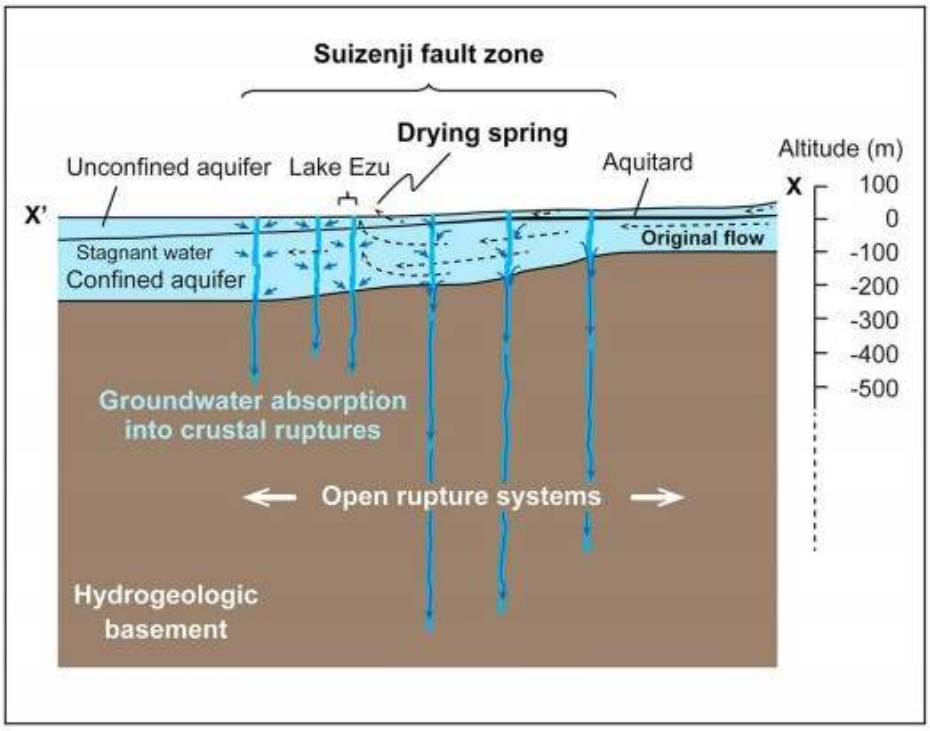

Figure 6. Cartoon showing hypothetical coseismic groundwater drawdown mechanism. Groundwater was transported downwards along crustal ruptures immediately after the main shock. The schematic hydrogeological cross-section is drawn between X-X′ in Figure 1b. Surface location of open ruptures is based on satellite radar interferometry (Fujiwara et al., 2016); depths are estimated from the present simulation.

The average hydraulic potential drop in the Suizenji fault area (n = 40; see Figure 2) within 35 min of the main shock was 0.83 m including both unconfined and confined aquifers. The missing groundwater volume under the Suizenji fault area, assuming that water dropped homogeneously over the region, is

$$V_{\text{missing groundwater}} = A \times L \times P, \quad (1)$$

where A, L, and P are the surface area of the Suizenji fault area (160 km^2), average water-level drop (0.83 m), and average porosity (0.2) of the aquifers, respectively. The calculation yielded a groundwater loss of 2.7 × 10^7 m^3. The hypothesized new volume of crustal ruptures within the Suizenji fault area ($V_{rupture}$) is calculated, assuming that the calculated volumetric expansion is accommodated by open cracks that extend homogenously to the deep crust:

$$V_{\text{rupture}} = A \times S \times D, \quad (2)$$

where S and D are the average volumetric strain change at well screens (2.45 × 10^{-5}, number of wells = 59) in the Suizenji fault area and the depth of crustal ruptures. Assuming that the missing groundwater fills the open ruptures, equations 1 and 2 imply that the crustal rupture extends to 6.8 km.

These calculations imply that the observed water drop can be explained by water drawdown through deep crustal ruptures to a depth of few kilometers. This depth is consistent with the reported focal depths of aftershocks under the Suizenji fault area, many of which have a normal-fault mechanism (Goto et al., 2017). However, this calculation does not include the effects of hydrogeological conditions, water pressure, or the location of the surface ruptures. To more precisely assess the effects of the pressurized water volume, we include surface-subsurface water interaction, groundwater flow, and the location of the rupture system in the GETFLOWS simulation (Mori et al., 2015). Very high hydraulic conductivities (1.0 cm/s) were assumed in the previously developed Kumamoto model (Hosono et al., 2013; Ichiyanagi et al., 2011; Mori et al., 2016; Shimada et al., 2012; see the supporting information) for the Suizenji fault systems (Figure S6). Observed (Fujiwara et al., 2016; Goto et al., 2017) and some estimated open structural deformations at the surface were extrapolated vertically to the deep crust (Figure S6). The depths of vertical ruptures associated with water flow were validated for each grid using reasonable fits between the observed and calculated groundwater drops for all monitoring sites in the Suizenji fault area (Figure S7). This fitting may be improved when anticipated additional rupture systems are more clearly defined by ongoing geophysical and geological surveys. The results are shown in Figure S6. The estimated depth of open ruptures associated with surface-subsurface water absorption and the total redistributed water volumes were ~5 km (Figure S6) and approximately 10^6 m^3, respectively. These values are smaller than those obtained from our idealized calculations because, in the latter, we did not account for the role of pore pressure redistribution. Because the vertical distribution and properties of the actual rupture systems are not known, our simulations cannot determine the actual depth of the ruptures that allowed water drawdown. Nevertheless, both results (idealized calculations and simulation) can qualitatively explain the observed water drop by water drawdown through crustal ruptures deeper than the confined and unconfined aquifers.

The model results show that estimated rupture depths are deepest in the eastern part of the Suizenji fault area (Figure 6) at the same location where the largest extensional volumetric strain occurred. In fact, the most active surface lateral displacements were identified in this region, deduced from satellite radar interferometry images and field surveys (Fujiwara et al., 2016; Goto et al., 2017; Lin, 2017; Lin & Chiba, 2017). Moreover, if the open-cracks are connected to the upper hydrological system, the water may be rapidly transported downward. The water-level decline was mostly completed within 35 min in wells (Figures 2 and 3), within 4 hr for spring discharge in Lake Suizenji, and within 12 hr for river discharge (Figure 5). These observations support the second hypothesis, the downward transport of meteoric water in shallow aquifers into new ruptures in the crust (Figure 6). The decrease in seismic velocity after the earthquake, monitored with ambient seismic noise, is consistent with the suggested fracturing of the upper 5 km of crust (Nimiya et al., 2017).

The third scenario, that surface water moved into dilatant cracks in the shallow crust formed by strong shaking, finds support from soil mechanics experiments. Since the 1960s, a great number of laboratory experiments have been carried out to study the mechanical response of unconsolidated sediments to earthquake shaking. These studies show that under cyclic shear loading, saturated unconsolidated sediments undergo nonelastic deformation such as volumetric contraction or expansion. Briefly, they may exhibit the following pattern of behavior (Elgamal et al., 2003): at low shear stress, the soil skeleton has a tendency for contraction, leading to development of excess pore-pressure and reduction in effective confinement; as shear stress approaches the failure envelope, the so-called phase transformation envelope (Elgamal et al., 2003) or the critical state envelope (Wang et al., 2001), contraction diminishes; at shear stress above the phase transformation envelop, soils may undergo continuous volumetric expansion (e.g., Elgamal et al., 2003; Luong, 1980). The transition from contraction to expansion occurs at a cyclic shear stress amplitude of ~0.2 MPa for medium grained sand (Luong, 1980).

Unconsolidated sediments in the study area exist only in the uppermost layer of alluvium or soft pyroclastic flow and ash deposits. The dilatant crack model may thus be strictly applicable only to the upper unconfined aquifer. The amplitude of the dynamic shear stress during the Kumamoto earthquake may be estimated from near-field ground motion records. Near-field ground motions were recorded at a seismic station (KMMH16; Fukuyama & Suzuki, 2016) located about 500 m northwest of the Futagawa fault (see Figure 1b for its location), both on the surface and at the bottom of a 252-m-deep borehole, with a peak ground acceleration (PGA) of 7 to 8 m/s^2 on the surface and ~2 m/s^2 at a depth of 252 m. Therefore, the average PGA may be ~7 m/s^2 for the upper unconfined aquifer and ~5 m/s^2 for the entire aquifer system. The average peak shear stress in the upper unconfined aquifer may be estimated from $\tau \approx \rho a z$ (Luong, 1980) where ρ is the average density of

the unconfined aquifer, a is the average PGA of the unconfined aquifer, and z is the average thickness of the unconfined aquifer. With an assumed average density of ~2,000 kg/m^3 for the upper unconfined aquifer, we estimate an average peak shear stress $\tau \approx 0.6$ MPa during the earthquake at the station. Thus, strong shaking in the Suizenji fault zone during the Kumamoto earthquake may have caused the upper unconfined aquifer to undergo volumetric dilatation.

Precise estimates of the amount of volumetric dilatation in this aquifer are hindered by the scarcity of field data. For an order of magnitude estimate, we may conservatively assume a volumetric expansion of 0.2% from laboratory experiments (e.g., Luong, 1980). Thus, given an average thickness of ~40 m for the upper unconfined aquifer (Figure 6), the volume of the dilatant cracks produced by seismic shaking is ~160 km^2 × 40 m × 0.2% = ~1.28 × 10^7 m^3, which is close in order of magnitude to the above estimates of the loss of water from the surface after the Kumamoto earthquake. Furthermore, the proximity of the surface water to the unconfined aquifer may easily account for the rapidity in the observed postseismic surface water response. Thus, the model of postseismic dilatancy of the shallow aquifers seems viable to account for the loss of surface water.

Both scenarios for transporting fluids though crustal ruptures and/or dilatant cracks can partly explain the observed water drawdown. If shallow dilatant cracks were the major driving force and if these cracks breached aquitards, water levels in deep confined aquifers would decrease (Wang et al., 2016). However, we have detected increased concentrations of organic matter and microorganisms in the deep confined aquifers, which originate from the surface environment but were not present before the earthquake (we will discuss details in other papers). It is a direct evidence of decreasing pressure below the unconfined aquifers and water transfer from the unconfined to confined aquifers or greater depths. Based on the spatial coincidence between water drawdown and rupture systems, we thus favor fluid transport though deep crustal ruptures to explain our observations.

The recovery of water levels by subsequent recharge was not completed until more than 45 days after the main shock, especially near the centre of the rupture zone (Figures 2c-2f and 3). This suggests that water absorbed in crustal openings was supplied from aquifers within and around the rupture zone (Figure 6). Water-level drops continued beyond the 35 min of the main shock in few wells (Figures 2d and 2f), suggesting continuous filling of new or existing open cracks. However, most of these anomalies were reduced after 1 year as a result of the annual hydrological cycle (Figures 2g and 2h). The spring also returned to its original flux. Water flow dynamics (Hosono et al., 2013; Kagabu et al., 2017; Ono et al., 2013), geochemical evolution (Hosono et al., 2014; Hossain et al., 2016; Hossain et al., 2016), anthropogenic pollution (Hosono et al., 2013), and microbiological features (Zeng et al.,

2016) have been intensively studied in the study area, and this information might provide additional insights into coseismic changes.

6 Implications and Summary

The most noteworthy finding of this study was the clear evidence of how an earthquake caused sudden groundwater drawdown. Similar water disappearance at Lake Suizenji was recorded at the time of the 1889 M 6.3 Kumamoto earthquake (reported by Yomiuri newspaper, 15 August 1889). Our results imply that coseismic water-level changes are useful in elucidating otherwise invisible features of seismic fault and rupture systems. In the extensional stress regime of Kyushu (Toda, 2016), bulk permeability is relatively high and groundwater can move downward through crustal ruptures where geothermal flows are too weak to trigger fluid expulsion (Sibson & Rowland, 2003). Our proposed model may be transferrable globally to the many other aquifer systems near convergent margins where volcanic rocks, alluvial deposits, and seismotectonics are co-located; it may also explain many observations where water-level decreases are not correlated with the volumetric strain near the fault zone (Chia et al., 2008; Cox et al., 2012; Muir-Wood & King, 1993; Wang & Chia, 2008).

Newly discovered coseismic hydrological changes imply chemical, isotopic, and microbiological changes as a result of the mixing of shallow water with deep groundwater. Moreover, increased seepage of waste water through damaged sewage pipes (Wells et al., 2013), and increased downward mobilization of anthropogenic pollutants (Hosono et al., 2013), can be expected. Our findings increase the global understanding of how earthquakes affect anthropogenic impacts on groundwater systems. These findings provide new understanding of the transport of dissolved materials and the subsequent management of ground water following disasters.

Acknowledgments

The authors declare no competing interests. The data used in this study are listed in figures and supporting information. The Government office of Kumamoto City, Kumamoto City Waterworks and Sewerage Bureau, Kumamoto Prefecture, and Ministry of Land, Infrastructure, Transport and Tourism kindly supplied water-level data. H. Suzuki and K. Ide are acknowledged for ground-surface level measurements. T. H. thanks the JSPS Grant-in-Aid for Scientific Research B (17H01861) and the SUNTORY Kumamoto groundwater research project for financial support. M. M. and C.-Y. W. are supported by NSF 1463997.

References

Brodsky, E. E., Roeloffs, E., Woodcock, D., Gall, I., & Manga, M. (2003). A mechanism for sustained ground water pressure changes induced by distant earthquakes. *Journal of Geophysical Research*, 108(B8), 2390. https://doi.org/10.1029/2002JB002321

Chia, Y., Chiu, J. J., Chiang, Y. -H., Lee, T. -P., Wu, Y. -M., & Horng, M. -J. (2008). Implications of coseismic groundwater level changes observed at multiple-well monitoring stations. *Geophysical Journal International*, 172(1), 293– 301. https://doi.org/10.1111/j.1365-246X.2007.03628.x

Cox, S. C., Rutter, H. K., Sims, A., Manga, M., Weir, J. J., Ezzy, T., White, P. A., Horton, T. W., & Scotte, D. (2012). Hydrological effects of the M_w 7.1 Darfield (Canterbury) earthquake, 4 September 2010, New Zealand. *New Zealand Journal of Geology and Geophysics*, 55(3), 231– 247. https://doi.org/10.1080/00288306.2012.680474

Elgamal, A., Yang, Z., Parra, Z., & Ragheb, A. (2003). Modeling of cyclic mobility in saturated cohesionless soils. *International Journal of Plasticity*, 19(6), 883– 905. https://doi.org/10.1016/S0749-6419(02)00010-4

Elkhoury, J. E., Brodsky, E. E., & Agnew, D. C. (2006). Seismic waves increase permeability. *Nature*, 441(7097), 1135– 1138. https://doi.org/10.1038/nature04798

Feuillet, N., Beauducel, F., Jacques, E., Tapponnier, P., Delouis, B., Bazin, S., Vallée, M., & King, G. C. P. (2011). The Mw = 6.3, November 21, 2004 Les Saintes earthquake (Guadeloupe): Tectonic setting, slip model and static stress changes. *Journal of Geophysical Research*, 116, B10301. https://doi.org/10.1029/2011JB008310

Fujiwara, S., Yarai, H., Kobayashi, T., Morishita, Y., Nakano, T., Miyahara, B., Nakai, H., Miura, Y., Ueshiba, H., Kakiage, Y., & Une, H. (2016). Small-displacement linear surface ruptures of the 2016 Kumamoto earthquake sequence detected by ALOS-2 SAR interferometry. *Earth, Planets and Space*, 68(1). https://doi.org/10.1186/s40623-016-0534-x

Fukuyama, E., & Suzuki, W. (2016). Near-fault deformation and Dc″ during the 2016 Mw7.1 Kumamoto earthquake. *Earth, Planets and Space*, 68(1), 194. https://doi.org/10.1186/s40623-016-0570-6

Goto, G., Tsutsumi, H., Toda, S., & Kumahara, Y. (2017). Geomorphic features of surface ruptures associated with the 2016 Kumamoto earthquake in and around the downtown of Kumamoto City, and implications on triggered slip along active faults. *Earth, Planets and Space*, 69(1). https://doi.org/10.1186/s40623-017-0603-9

Hosono, T., Tokunaga, T., Kagabu, M., Nakata, H., Orishikida, T., Lin, I. -T., & Shimada, J. (2013). The use of $\delta^{15}N$ and $\delta^{18}O$ tracers with an understanding of groundwater flow dynamics for evaluating the origins and attenuation mechanisms of nitrate pollution. *Water Research*, 47(8), 2661– 2675. https://doi.org/10.1016/j.watres.2013.02.020

Hosono, T., Tokunaga, T., Tsushima, A., & Shimada, J. (2014). Combined use of $\delta^{13}C$, $\delta^{15}N$, and $\delta^{34}S$ tracers to study anaerobic bacterial processes in groundwater flow systems. *Water Research*, 54, 284– 296. https://doi.org/10.1016/j.watres.2014.02.005

Hossain, S., Hosono, T., Ide, K., Matsunaga, M., & Shimada, J. (2016). Redox processes and occurrence of arsenic in a volcanic aquifer system of Kumamoto Area, Japan. *Environmental Earth Sciences*, 75(9), 740. https://doi.org/10.1007/s12665-016-5557-x

Hossain, S., Hosono, T., Yang, H., & Shimada, J. (2016). Geochemical processes controlling fluoride enrichment in groundwater at the western part of Kumamoto area, Japan. *Water, Air, & Soil Pollution*, 227(10), 385. https://doi.org/10.1007/s11270-016-3089-3

Ichiyanagi, K., Shimada, J., Kagabu, M., Saita, S., & Mori, K. (2012) Simulations of tritium age and $\delta^{18}O$ distributions in groundwater by using surface-subsurface coupling full-3D distribution model (GETFLOWS) in Kumamoto, Japan. 39th Congress of the International Association of Hydrogeologists (IAH), Sheraton on the Falls Conference Centre, Ontario, Canada. Abstract ID, 280.

Jónsson, S., Segall, P., Pedersen, R., & Björnsson, G. (2003). Post-earthquake ground movements correlated to pore-pressure transients. *Nature*, 424(6945), 179– 183. https://doi.org/10.1038/nature01776

Kagabu, M., Matsunaga, M., Ide, K., Momoshima, N., & Shimada, J. (2017). Groundwater age determination using ^{85}Kr and multiple age tracers (SF_6, CFCs, and ^{3}H) to elucidate regional groundwater flow systems. *Journal of Hydrology: Regional Studies*, 12, 165– 180. https://doi.org/10.1016/j.ejrh.2017.05.003

Kitamura, A., Kurikami, H., Sakuma, K., Malins, A., Okumura, M., Machida, M., Mori, K., Tada, K., Tawara, Y., Kobayashi, T., Yoshida, T., & Tosaka, H. (2016). Redistribution and export of contaminated sediment within eastern Fukushima Prefecture due to typhoon flooding. *Earth Surface Processes and Landforms*, 41(12), 1708– 1726. https://doi.org/10.1002/esp.3944

Lai, W.-C., Koizumi, N., Matsumoto, N., Kitagawa, Y., Lin, C.-W., Shieh, C.-L., & Lee, U.-P. (2004). Effects of seismic ground motion and geological setting on the coseismic groundwater level changes caused by the 1999 Chi-Chi earthquake, Taiwan. *Earth, Planets and Space*, 56(9), 873– 880. https://doi.org/10.1186/BF03352534

Lin, A. (2017). Structural features and seismotectonic implications of coseismic surface ruptures produced by the 2016 M_w 7.1 Kumamoto earthquake. *Journal of Seismology*, 21(5), 1079– 1100. https://doi.org/10.1007/s10950-017-9653-5

Lin, A., & Chiba, T. (2017). Coseismic conjugate faulting structures produced by the 2016 M_w 7.1 Kumamoto earthquake, Japan. *Journal of Structural Geology*, 99, 20– 30. https://doi.org/10.1016/j.jsg.2017.05.003

Luong, M. P. (1980). Stress-strain aspects of cohesionless soils under cyclic and transient loading. In G. N. Pande & O. C. Zienkiewicz (Eds.), *Proceeding*

of International Symposium of Soils under Cyclic and Transient Loading (pp. 315– 321). Rotterdam, Netherlands: A. A. Balkema.

Manga, M., & Wang, C. -Y. (2015). Earthquake hydrology. In G. Schubert (Ed.), *Treatise on Geophysics* (pp. 305– 328). Oxford: Elsevier. https://doi.org/10.1016/B978-0-444-53802-4.00082-8

Matsumoto, S., Nishimura, T., & Ohkura, T. (2016). Inelastic strain rate in the seismogenic layer of Kyushu Island, Japan. *Earth, Planets and Space*, 68(1), 207. https://doi.org/10.1186/s40623-016-0584-0

Mohr, C. H., Manga, M., Wang, C.-Y., & Korup, O. (2017). Regional changes in streamflow after a megathrust earthquake. *Earth and Planetary Science Letters*, 458, 418– 428. https://doi.org/10.1016/j.epsl.2016.11.013

Montgomery, D. R., & Manga, M. (2003). Streamflow and water well responses to earthquakes. *Science*, 300(5628), 2047– 2049. https://doi.org/10.1126/science.1082980

Mori, K., Tada, K., Tawara, Y., Ohno, K., Asami, M., Kosaka, K., & Tosaka, H. (2015). Integrated watershed modeling for simulation of spatiotemporal redistribution of post-fallout radionuclides: Application in radiocesium fate and transport processes derived from the Fukushima accidents. *Environmental Modelling & Software*, 72, 126– 146. https://doi.org/10.1016/j.envsoft.2015.06.012

Mori, K., Tawara, Y., Tada, K., Hosono, T., Shimada, J., Matsunaga, M., & Tosaka, H. (2016). Numerical modeling for simulating fate and reactive transport processes of nitrogen in watershed and discussion on applicability to actual fields. *Journal of Groundwater Hydrology*, 58(1), 63– 86 (in Japanese with English abstract). https://doi.org/10.5917/jagh.58.63

Muir-Wood, R., & King, G. C. P. (1993). Hydrological signatures of earthquake strain. *Journal of Geophysical Research*, 98(B12), 22,035– 22,068. https://doi.org/10.1029/93JB02219

Nimiya, H., Ikeda, T., & Tsuji, T. (2017). Spatial and temporal seismic velocity changes on Kyushu Island during the 2016 Kumamoto earthquake. *Science Advances*, 3(11), e1700813. https://doi.org/10.1126/sciadv.1700813

Okada, Y. (1992). Internal deformation due to shear and tensile faults in a half-space. *Bulletin of the Seismological Society of America*, 82(2), 1018–1040.

Ono, M., Tokunaga, T., Shimada, J., & Ichiyanagi, K. (2013). Application of continuous ^{222}Rn monitor with dual loop system in a small lake. *Groundwater*, 51(5), 706– 713. https://doi.org/10.1111/gwat.12002

Pliny, (n.d.) the Elder, ca. AD 77-79. The Natural History.

Rojstaczer, S., & Wolf, S. (1992). Permeability changes associated with large earthquakes: An example from Loma Prieta, California. *Geology*, 20(3), 211–214. https://doi.org/10.1130/0091-7613(1992)020<0211:PCAWLE>2.3.CO;2

Rojstaczer, S., Wolf, S., & Michel, R. (1995). Permeability enhancement in the shallow crust as a cause of earthquake-induced hydrological processes. *Nature*, 373(6511), 237– 239. https://doi.org/10.1038/373237a0

Sakuma, K., Kitamura, A., Malins, A., Kurikami, H., Machida, M., Mori, K., Tada, K., Kobayashi, T., Tawara, Y., & Tosaka, H. (2017). Characteristics of radio-cesium transport and discharge between different basins near to the Fukushima Dai-ichi Nuclear Power Plant after heavy rainfall events. *Journal of Environmental Radioactivity*, 169-170, 137– 150. https://doi.org/10.1016/j.jenvrad.2016.12.006

Sano, Y., Takahata, N., Kagoshima, T., Shibata, T., Onoue, T., & Zhao, D. (2016). Groundwater helium anomaly reflects strain change during the 2016 Kumamoto earthquake in Southwest Japan. *Scientific Reports*, 6(1), 37939. https://doi.org/10.1038/srep37939

Sato, T., Sakai, R., Furuya, K., & Kodama, T. (2000). Coseismic spring flow changes associated with the 1995 Kobe earthquake. *Geophysical Research Letters*, 27(8), 1219– 1222. https://doi.org/10.1029/1999GL011187

Shi, Z., Wang, G., Manga, M., & Wang, C. -Y. (2015). Permeability changes after large earthquakes: insights from co-seismic water level changes throughout China in response to four M>8 earthquakes. *Earth and Planetary Science Letters*, 430, 66– 74. https://doi.org/10.1016/j.epsl.2015.08.012

Shimada, J., Ichiyanagi, K., Kagabu, M., Saita, S., & Mori, K. (2012) Evaluation of long-term artificial groundwater recharge through leaky rice paddies with a 500 year history. 39th Congress of the International Association of Hydrogeologists (IAH), Sheraton on the Falls Conference Centre, Ontario, Canada. Abstract ID, 232.

Sibson, R. H., & Rowland, J. V. (2003). Stress, fluid pressure and structural permeability in seismogenic crust, North Island, New Zealand. *Geophysical Journal International*, 154(2), 584– 594. https://doi.org/10.1046/j.1365-246X.2003.01965.x

Taniguchi, M., Burnett, K., Shimada, J., Hosono, T., Wada, C. A., & Ide, K. (2019). Recovery of lost nexus synergy via payment for environmental services in Kumamoto, Japan. *Frontiers in Environmental Science*, 7, 28. https://doi.org/10.3389/fenvs.2019.00028

Tawara, Y., Hazart, A., Mori, K., Tada, K., Shimura, T., Sato, S., Yamamoto, S., Asano, H., & Namiki, K. (2014). Extended two-phase flow model with mechanical capability to simulate gas migration in bentonite. *Geological Society, London, Special Publications*, 400, 545– 562. https://doi.org/10.1144/SP400.7

Toda, S. (2016). Crustal earthquakes. In T. Moreno, S. Wallis, T. Kojima, & W. Gibbons (Eds.), *The Geology of Japan*, Geological Society (pp. 371– 408). London.

Tsunogai, U., & Wakita, H. (1995). Precursory chemical changes in ground water: Kobe earthquake, Japan. *Science*, 269(5220), 61– 63. https://doi.org/10.1126/science.269.5220.61

Wakamatsu, K., Senna, S., & Ozawa, K. (2017). Liquefaction and its characteristics during the 2016 Kumamoto earthquake. *Journal of Japan Association for Earthquake Engineering*, 17(4), 4_81– 4_100 (in Japanese with English abstract). https://doi.org/10.5610/jaee.17.4_81

Wakita, H. (1975). Water wells as possible indicators of tectonic strain. *Science*, 189(4202), 553– 555. https://doi.org/10.1126/science.189.4202.553

Wang, C. -Y., & Barbour, A. J. (2017). Influence of pore pressure change on coseismic volumetric strain. *Earth and Planetary Science Letters*, 475, 152–159. https://doi.org/10.1016/j.epsl.2017.07.034

Wang, C. -Y., Cheng, L. -H., Chin, C. -V., & Yu, S. -B. (2001). Coseismic hydrologic response of an alluvial fan to the 1999 Chi-Chi earthquake, Taiwan. *Geology*, 29(9), 831– 834. https://doi.org/10.1130/0091-7613(2001)029<0831:CHROAA>2.0.CO;2

Wang, C. -Y., & Chia, Y. (2008). Mechanism of water level changes during earthquakes: Near field versus intermediate field. *Geophysical Research Letters*, 35, L12402. https://doi.org/10.1029/2008GL034227

Wang, C. -Y., Liao, X., Wang, L. -P., Wang, C. -H., & Manga, M. (2016). Large earthquakes create vertical permeability by breaching aquitards. *Water Resources Research*, 52, 5923– 5937. https://doi.org/10.1002/2016WR018893

Wang, C.-Y., & Manga, M. (2015). New streams and springs after the 2014 M_w 6.0 South Napa earthquake. *Nature Communications*, 6(7597). https://doi.org/10.1038/ncomms8597

Wang, C. -Y., Wang, C. H., & Manga, M. (2004). Coseismic release of water from mountains: Evidence from the 1999 (Mw¼7.5) Chi-Chi earthquake. *Geology*, 32(9), 769– 772. https://doi.org/10.1130/G20753.1

Wells, N. S., Clough, T. J., Condron, L. M., Baisden, W. T., Harding, J. S., Dong, Y., Lewis, G. D., & Lear, G. (2013). Biogeochemistry and community ecology in a spring-fed urban river following a major earthquake. *Environmental Pollution*, 182, 190– 200. https://doi.org/10.1016/j.envpol.2013.07.017

Wessel, P., & Smith, W. H. F. (1998). New, improved version of generic mapping tools released. *EOS, Transactions, American Geophysical Union*, 79(47). https://doi.org/10.1029/98EO00426

Yano, T. E., & Matsubara, M. (2017). Effect of newly refined hypocenter locations on the seismic activity recorded during the 2016 Kumamoto Earthquake sequence. *Earth, Planets and Space*, 59(74). https://doi.org/10.1186/s40623-017-0656-9

Yarai, H., Kobayashi, T., Morishita, Y., Fujiwara, S., Hiyama, Y., Kawamoto, S., Ueshiba, H., Miura, Y., & Miyahara, B. (2016). Source fault models of the 2016 Kumamoto earthquake inverted from crustal deformation. *Journal of Geospatial Information Authority of Japan*, 128, 169– 176. (in Japanese)

Zeng, X., Hosono, T., Ohta, H., Niidome, T., Shimada, J., & Morimura, S. (2016). Comparison of microbial communities inside and outside of a denitrification hotspot in confined groundwater. *International Biodeterioration & Biodegradation*, 114, 104– 109. https://doi.org/10.1016/j.ibiod.2016.05.019